PNAS
www.pnas.org

Supplementary Information for

Muscle-like Fatigue-resistant Hydrogels by Mechanical Training

Shaoting Lin, Ji Liu, Xinyue Liu, Xuanhe Zhao[†]

[†]Email: zhaox@mit.edu

This PDF file includes:

Supplementary text
Table S1
Figs. S1 to S12
Caption for movie S1
References for SI reference citations

Other supplementary materials for this manuscript include the following:

Movie S1

Supplementary Information Text

www.pnas.org/cgi/doi/10.1073/pnas.1903019116

Materials and Methods

Materials. All PVA hydrogels (i.e., chemically cross-linked, freeze-thawed, and prestretched PVA hydrogels) were synthesized from a 10 wt% poly(vinyl alcohol) (PVA; Mw 146,000-186,000, 99+% hydrolyzed; Sigma-Aldrich, 363065) solution. The solution was heated in a water bath at 100 °C with stirring for 5 hours. To synthesize the chemically cross-linked PVA hydrogel, we added 10 μL glutaraldehyde (25 vol%, Sigma-Aldrich, G6257) as a cross-linker to a 1 mL 10 wt% PVA solution, and added 10 μL hydrochloric acid (36.5-38 wt%, J.T. Baker, 9535-02) as an accelerator into the other 1 mL of 10 wt% PVA solution. We then mixed and defoamed each solution by using a centrifugal mixer (AR-100; Thinky). The final mixtures obtained by mixing then defoaming the two solutions were then casted into a mold and allowed to cure for 2 hours. The chemically cross-linked PVA hydrogel was immersed in deionized water for two days to remove unreacted chemicals. To fabricate the freeze-thawed PVA hydrogel, 10 wt% PVA solutions after mixing and defoaming were poured into a mold, frozen at -20 °C for 8 hours then thawed at 25 °C for 3 hours. The freeze-thawing process was repeated five times. To fabricate the prestreched PVA hydrogel, we cyclically prestretched the freeze-thawed hydrogel in a water bath using a mechanical stretcher (Cellscale, Canada). The sufficiently aligned nanofibrils were achieved by applying the maximum applied stretch of 4.6 for 1000 cycles.

Confocal imaging of PVA hydrogels in wet state. To visualize the microstructures of the PVA hydrogels, a fluorescent dye, 5-([4,6-dichlorotriazin-2-yl]amino)fluorescein hydrochloride (5-DTAF), was used to label the PVA side groups (Fig. S1). Specifically, PVA hydrogel samples were first immersed in a large volume of sodium bicarbonate solution (0.1 M, pH 9.0) for 12 hours to equilibrate the pH within the samples. 5 mg of 5-DTAF dissolved in 1.0 mL of anhydrous dimethyl sulfoxide (DMSO) was further added into 100 mL of the sodium bicarbonate solution

(0.1 M, pH 9.0) to form a reactive dye solution. The pH-equilibrated PVA samples were immersed in the dye solution for 12 hours at 4 °C in a dark environment to form conjugated fluorochromes. Finally, the hydrogel samples were rinsed several times with deionized water to wash away the non-conjugated dyes, prior to fluorescence imaging. The hydrogel microstructures were imaged using a confocal microscope (Leica TCS SP8). Laser intensity, filter sensitivity, and grayscale threshold were adjusted in each application to optimize the contrast of the images. *In situ* fluorescent imaging of the PVA hydrogel samples during uniaxial stretching was conducted using a linear stretcher (Micro Vice Holder, STJ-0116).

X-ray scattering. We investigated nanocrystalline morphologies in nanofibrils of freeze-thawed PVA hydrogels before and after the prestretches through small angle X-ray scattering (SAXS). The X-ray scattering measurements were performed with a Pilatus3R 300K detector (Bruker Nanostar SAXS in X-ray diffraction shared experimental facility). The measured scattering intensity I of PVA hydrogels in the swollen state was corrected by subtracting the water background. A customized linear stretcher was designed to hold the samples at the various stretches for *in situ* X-ray scattering measurements.

SEM imaging. The SEM images were acquired with supercritically-dried samples by a scanning electron microscope (JEOL 5910). We followed the reported experimental protocol to probe the nanoscale structures of the prestretched PVA (1). A notched sample was gradually elongated to a stretch of 2 without obvious crack propagation in order to delaminate the fibrils near the notch. The PVA sample was immediately immersed in a 2.5 wt% glutaraldehyde solution for 3 hours to fix the structure, and dehydrated through a series of alcohol solutions in ascending concentration (30, 50, 70, 90, 95, and 100 vol% twice) in order to avoid non-uniform shrinkage. The dehydrated PVA sample was fractured along the notch using forceps immediately after being

frozen in liquid nitrogen. The fractured samples were kept in ethanol and dried in a supercritical dryer (Automegasamdri Series C, Tousimis). The dried fracture surfaces were then sputter coated with gold and observed by SEM (JEOL 5910).

AFM phase imaging. AFM phase images were acquired with an atomic force microscope (MFP-3D, Asylum Research) in tapping mode. Dry freestanding PVA films were directly attached onto the sample stage with double-sided carbon tape. The probe lightly tapped on the sample surface with a recorded phase shift angle of the probe motion relative to a driving oscillator. The bright regions with high phase angles correspond to regions with a relatively high modulus, and the dark regions with low phase angles correspond to regions with a relatively low modulus.

Mechanical characterization. All the mechanical tests were performed in a water bath at 25°C with a U-stretch testing device (CellScale, Canada). For mechanically weak samples (e.g., the chemically cross-linked hydrogel), a load cell with a maximum force of 4.4 N was used; for mechanically strong samples (e.g., the freeze-thawed and prestretched PVA hydrogels), a load cell with a maximum force of 44 N was used. The nominal stress S was measured from the recorded force F divided by width W and thickness t in the swollen state. The stretch was calculated by the applied displacement divided by gauge length of the sample at undeformed state. The Young's modulus was calculated from the initial slope of the nominal stress versus stretch curve. The ultimate tensile strength was identified at the maximum nominal stress when the sample ruptures.

To measure the fatigue threshold of PVA hydrogels, we adopted the single-notch method, which is widely used in fatigue tests of rubbers. All fatigue tests in this study were performed on fully swollen hydrogels immersed in a water bath to prevent the dehydration-induced crack propagation. Cyclic tensile tests were conducted on notched and unnotched samples with identical dogbone shapes. The initial crack length in notched sample was smaller than one-fifth of the width

of the sample. The curves of nominal stress S versus stretch λ of the unnotched samples were obtained over Nth cycles with the maximum applied stretch of λ_{max}. The strain energy density of the unnotched sample under the Nth cycle with the maximum applied stretch of λ_{max} can be calculated as $W(\lambda_{max}, N) = \int_1^{\lambda_{max}} S d\lambda$. Thereafter, the same maximum applied stretch λ_{max} was applied on the notched sample, and we recorded the crack length at the undeformed state c over cycles using a digital microscope (AM4815ZT, Dino-Lite; resolution, 20 mm/pixel). The applied energy release rate G in the notched sample under the Nth cycle with the maximum applied stretch of λ_{max} can be calculated as $G(\lambda_{max}, N) = 2k(\lambda_{max}) \cdot c(N) \cdot W(\lambda_{max}, N)$, where k is a slowly varying function of the applied stretch as $k = 3/\sqrt{\lambda_{max}}$. By varying the applied stretch of λ_{max}, we acquired the curve of crack extension per cycle dc/dN versus the applied energy release rate G. The fatigue threshold can be obtained by linearly extrapolating the curve of dc/dN vs. G to the intercept with the abscissa. Considering the resolution of the camera is around 0.02 mm (20 μm/pixel for the camera), the detectable resolution of dc/dN is 0.002 μm/cycle for our setup, which is on the same order as the resolution in previous fatigue tests for fatigue thresholds of rubbers (i.e., 0.001 μm/cycle) (2). Unlike bulk PVA samples, there was no detectable fatigue-crack propagation in 3D-printed micro-meshes with a notch (that is, if the crack does not propagate during the 1st cycle in the 3D-printed micro-meshes, it will not propagate over subsequent cycles unless a higher stretch is applied), possibly because the filaments were trained and became stronger during cyclic fatigue measurements. This observation was consistent with the recent work on the design of stretchable materials with high toughness and high resilience (3).

Measurement of water content. We measured the water content in swollen PVA hydrogels using thermal gravimetric analysis (furnace: TGA1-0075, control unit: DCC1-00177). We first cut a disk

shape of swollen PVA hydrogels of 3-7 mg. The swollen hydrogels weighing $m_{swollen}$ in a titanium pan without any water droplet on the surface of the samples. The samples were thereafter heated up from 30 °C to 150 °C at the rate of 20 °C/min, and then 150 °C to 160 °C at the rate of 5 °C/min under a nitrogen atmosphere at a flow rate of 30 mL/min. The measured mass of the sample was recorded. In Fig. S7, a typical TGA curve of pristine freeze-thawed PVA hydrogels is plotted. The mass of the sample decreases with the increase of temperature and gradually reaches a plateau m_{dry} when the all residual water in the sample evaporates. The water contents of the swollen PVA hydrogels ϕ_{water} were identified using $1-m_{dry}/m_{swollen}$.

Measurement of crystallinities. We measured the crystallinities of the resultant PVA hydrogels using differential scanning calorimetry (DSC/cell: RCS1-3277, cooling system: DSC1-0107), following the experimental protocols in the paper (4). Before air-drying the PVA hydrogels for DSC measurements, we first used excess chemical cross-links to fix the amorphous polymer chains to minimize the further formation of crystalline domains during the air-drying process. Specifically, we soaked the samples (thickness of 1 mm) in the aqueous solution consisting of 10 mL of glutaraldehyde (25 vol%;), 500 μL of hydrochloric acid (36.5 to 38 wt%), and 100 mL of DI water for 1 hour. Thereafter, we soaked the samples in a deionized water bath for 1 hour to remove the extra glutaraldehyde and hydrochloric acid. The samples were further dried in an incubator (New Brunswick Scientific, C25) at 37 °C for 1 hour.

In a typical DSC measurement, we first weighed the total mass of the air-dried sample *m* (still with residual water). The sample was thereafter placed in a Tzero pan and heated up from 50 °C to 250 °C at the rate of 20 °C/min under a nitrogen atmosphere with flow rate of 30 mL/min. The curve of heat flow shows a broad peak from 60 °C to 180 °C, indicating that the air-dried sample contained a small amount of residual water. The integration of the endothermic transition

ranging from 60 °C to 180 °C gives the enthalpy for evaporation of the residual water per unit mass of the dry sample (with residual water) $H_{residual}$. Therefore, the mass of the residual water $m_{residual}$ can be calculated as $m_{residual} = m \cdot H_{residual} / H^0_{water}$, where $H^0_{water} = 2260$ J/g is the latent heat of water evaporation. The curve of heat flow shows another narrow peak ranging from 200 °C to 250 °C, corresponding to the melting of the crystalline domains. The integration of the endothermic transition ranging from 200 °C to 250 °C gives the enthalpy for melting the crystalline domains per unit mass of the dry sample (with residual water) $H_{crystalline}$. Therefore, the mass of the crystalline domains $m_{crystalline}$ can be calculated as $m_{crystalline} = m \cdot H_{crystalline} / H^0_{crystalline}$, where $H^0_{crystalline} = 138.6$ J/g is the enthalpy of fusion of 100 wt.% crystalline PVA measured at the equilibrium melting point T^0_m (5). Therefore, the crystallinity in the ideally dry sample X_{dry} (without residual water) can be calculated as $X_{dry} = m_{crystalline} / \left(m - m_{residual}\right)$. With measured water content from TGA, the crystallinity in the swollen state can be calculated as $X_{swollen} = X_{dry} \cdot \left(1 - \phi_{water}\right)$.

3D printing meshes of PVA hydrogels. The microstructures of PVA hydrogels were fabricated by printing a 3D structure onto a glass slide (Corning). Print paths were generated via production of G-code that controls the XYZ motion of the 3D robotic gantry (Aerotech). G-code was either generated by manual coding or open-source software (Slic3r). The prepared PVA inks were stored in 5 mL syringe barrels, which fitted the nozzles with diameters of 400 μm (EFD Nordson). To achieve stable and optimal printing, we chose 50 kPa of air pressure (Ultimus V, Nordson EFD) as the printing pressure, and 15 wt% PVA (146 kDa, 99% hydrolysis ratio) aqueous solution as the printing ink. After deposition, the printed samples underwent five cycles of freezing (-20 °C for 8 hours) and thawing (20 °C for 3 hours) to achieve the final PVA hydrogel meshes. The

prestretched PVA meshes were acquired by applying cyclic prestretching of 3.5 over 1000 cycles on the dogbone-shaped pristine mesh in both in-plane directions.

	Strain-stiffening hydrogels[6,7]	Bottlebrush elastomers[8,9]	Tough hydrogels[10,11]	Hydrogel composites[12,13]	Nanocrystalline hydrogels[3]	Muscle-like hydrogels
E (kPa) Young's modulus	0.01-0.5	1-100	10-100	1000-10,000	1000-10,000	200
W (wt %) Water content	> 99	0	90	60-80	60-70	84
S (kPa) Nominal strength	~ 0.2	10-100	100-1000	1000-10,000	4000-10,000	5200
Γ_0 (J/m^2) Fatigue threshold	~ 1	~ 10	50-400	~ 1000	400-1000	1250

Table S1. Comparison of combinational properties in various soft materials. Comparison of Young's moduli, water contents, nominal strengths, and fatigue thresholds of strain-stiffening hydrogels (6, 7), bottlebrush elastomers (8, 9), tough hydrogels (10, 11), hydrogel composites (12, 13), nanocrystalline hydrogels (4), and muscle-like hydrogels in this work.

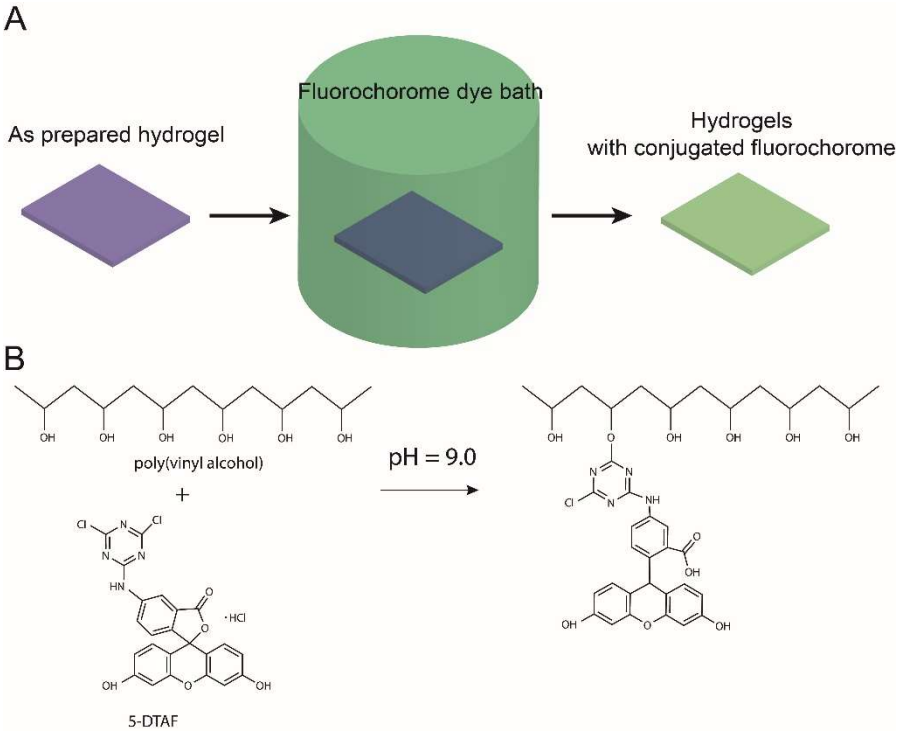

Fig. S1. Conjugation of fluorochoromes on PVA for confocal imaging. *(A)* The fabrication method to introduce conjugated fluorochoromes on PVA polymer chains. *(B)* The chemical reaction for conjugation of fluorochorome on PVA.

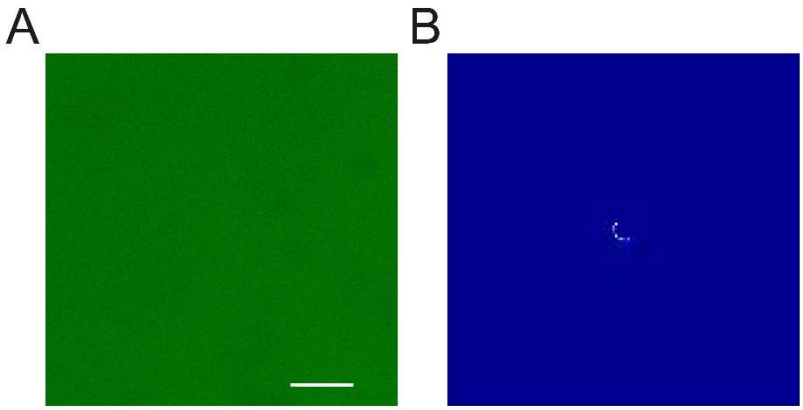

Fig. S2. Morphology characterization of chemically cross-linked PVA hydrogel. *(A)* Confocal image. *(B)* SAXS pattern.

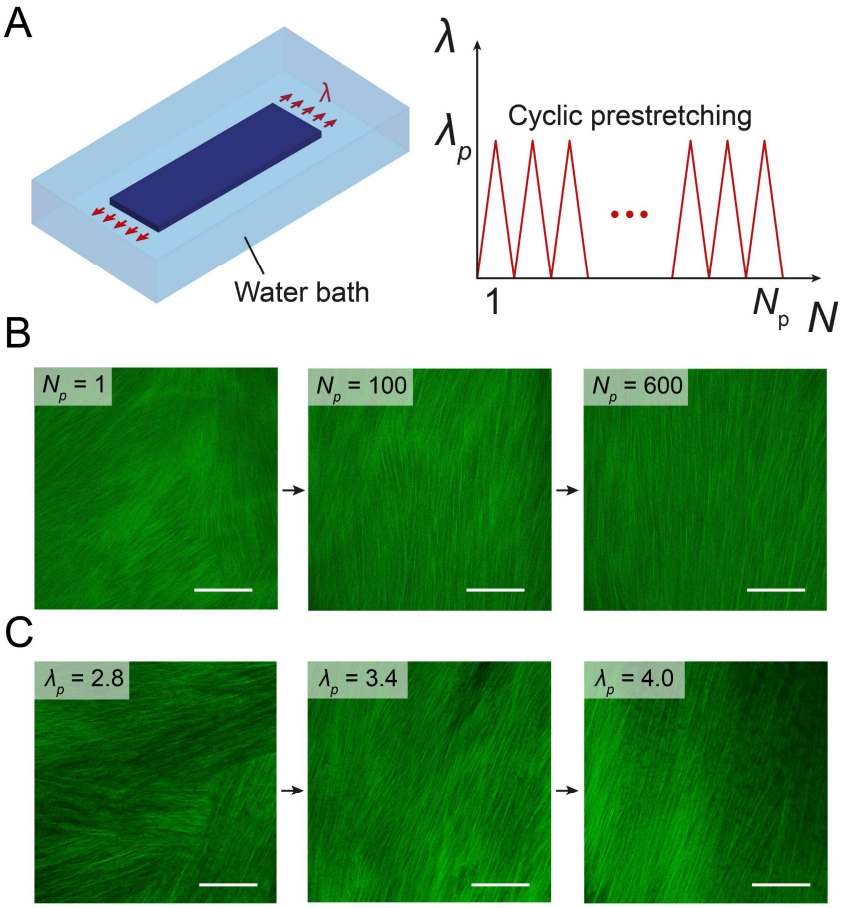

Fig. S3. The effect of applied prestretch and cycle number on the alignment of nanofibrils in PVA hydrogels. *(A)* Schematic illustration of mechanical training of hydrogels to form aligned nanofibrils. *(B)* Confocal images of the PVA hydrogels after 1, 100 and 600 cycles of prestretches of 4.6. *(C)* Confocal images of the PVA hydrogels after 1000 cycles of prestretches of 2.8, 3.4 and 4.0.

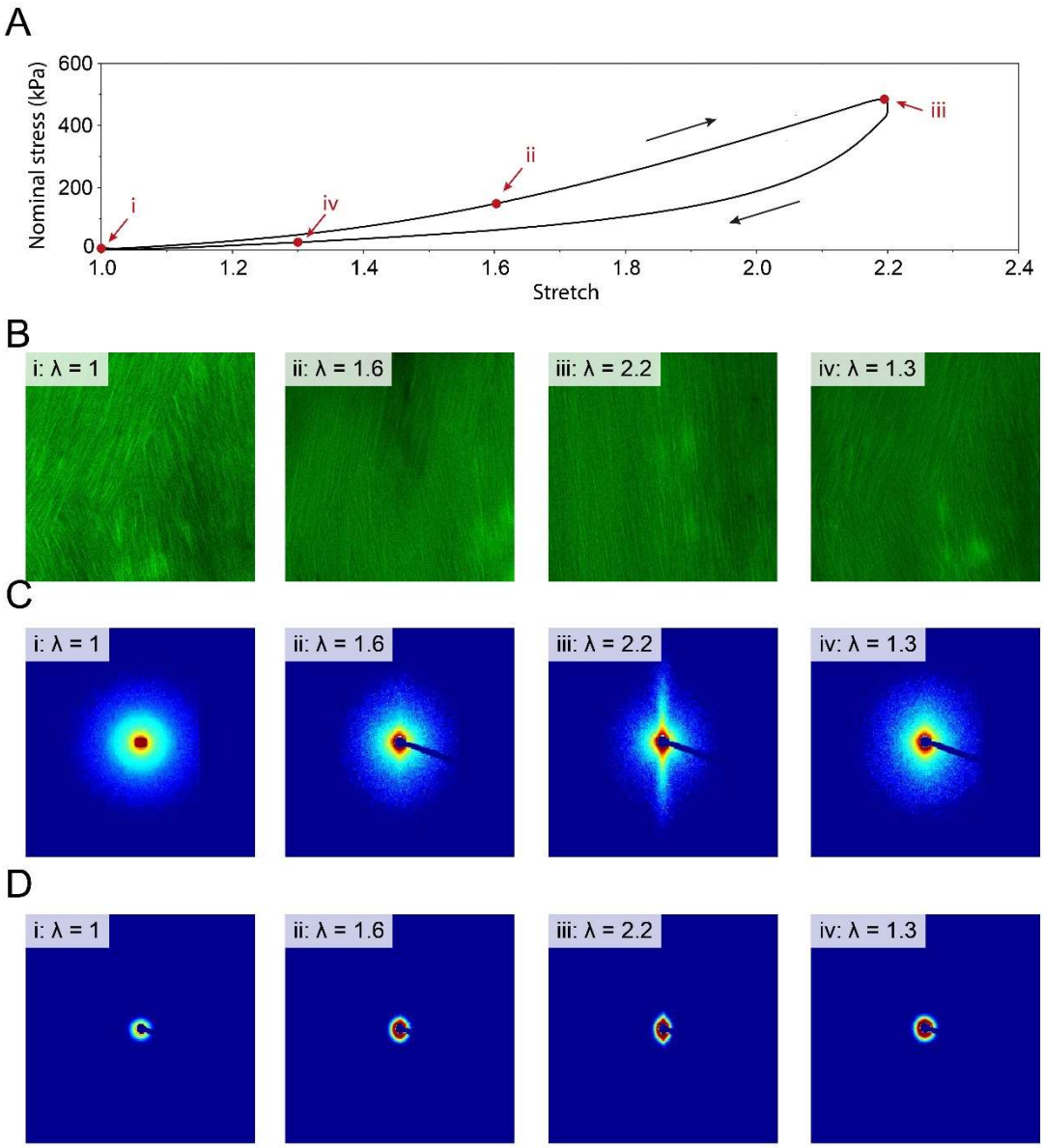

Fig. S4. Confocal images, SAXS, and WAXS patterns of the freeze-thawed PVA hydrogel under a single cycle of load. *(A)* Representative stress vs. stretch curve of the freeze-thawed PVA hydrogel. *(B)* Confocal images, *(C)* SAXS patterns, and *(D)* WAXS patterns of the freeze-thawed PVA hydrogel at the applied stretch of i: $\lambda = 1$, ii: $\lambda = 1.6$, iii: $\lambda = 2.2$ under loading and at the applied stretch of iv: $\lambda = 1.3$ under unloading.

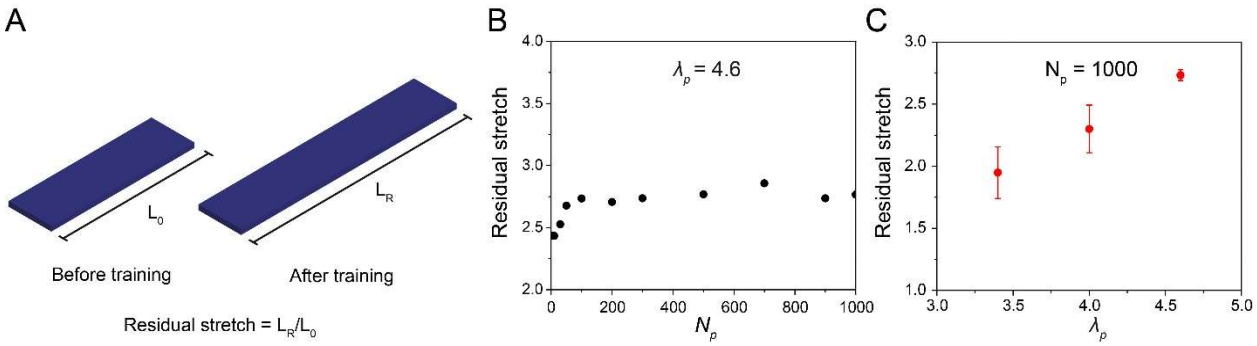

Fig. S5. Residual stretch of prestretched PVA hydrogels. *(A)* The residual stretch is defined as the ratio of the length at undeformed state after training L_R over the length at undeformed state before training L_0. *(B)* Residual stretch after N_p cycles of applied prestretches of 4.6. *(C)* Residual plastic stretch after 1000 cycles of prestretches of λ_p.

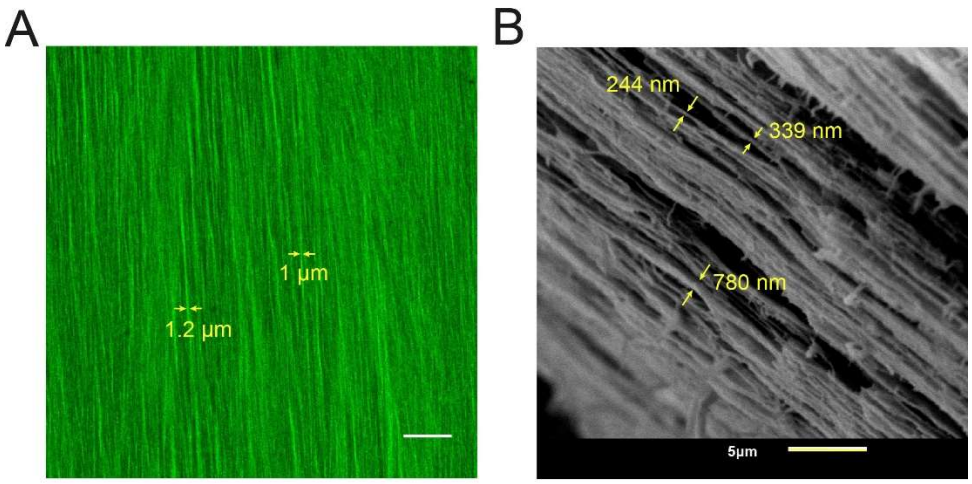

Fig. S6. Measurement of nanofibril diameters in the prestretched PVA hydrogel. *(A)* Confocal image. *(B)* SEM image. The sample for SEM imaging was first mechanically stretched to induce delamination of nanofibrils, and immediately crosslinked by glutaraldehyde to avoid further collapse during supercritical drying, followed by SEM observation. The measured diameters of aligned nanofibrils in the hydrogel range from ~100 nm to ~1 μm. Scale bar is 20 μm in *(A)* and 5 μm in *(B)*.

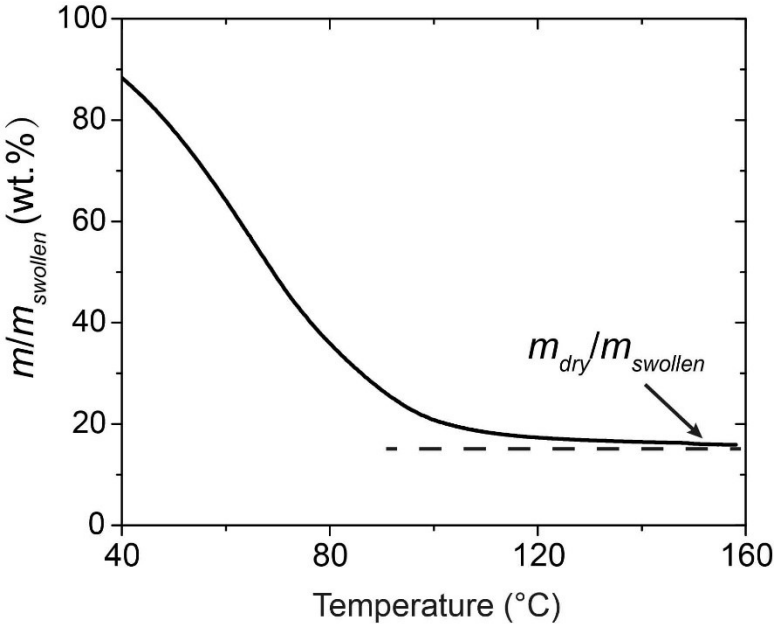

Fig. S7. Representative thermal gravimetric analysis (TGA) curve of the freeze-thawed PVA hydrogel. m, m_{swollen}, and m_{dry} denote the mass of the sample during TGA measurement, in the swollen state, and in fully dry state, respectively.

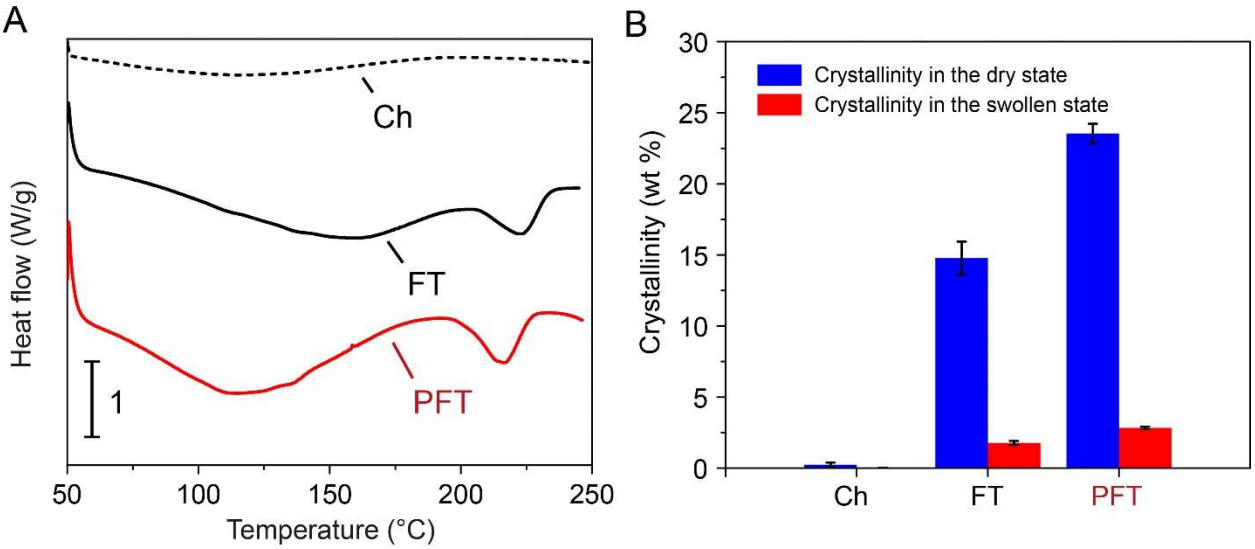

Fig. S8. Measurement of crystallinities in PVA hydrogels. *(A)* Differential scanning calorimetry (DSC) thermographs of chemically cross-linked (i.e., Ch), freeze-thawed (i.e., FT), and prestretched PVA hydrogels (i.e., PFT). *(B)* Summarized crystallinities in the dry state and crystallinities in the swollen state of Ch, FT, and PFT hydrogels.

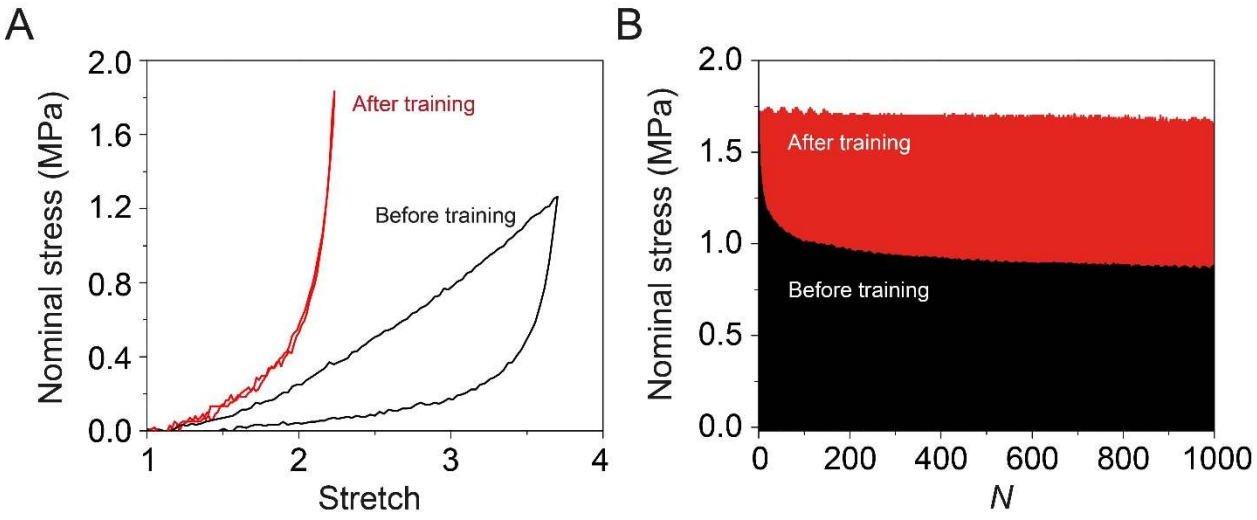

Fig. S9. Comparison of hysteresis in PVA hydrogels before and after mechanical training. *(A)* Loading-unloading nominal stress versus stretch curves of PVA hydrogels before and after training. *(B)* Nominal stress over loading cycles of PVA hydrogels before and after training with maximum applied stretch of 4.5 and 2.2, respectively.

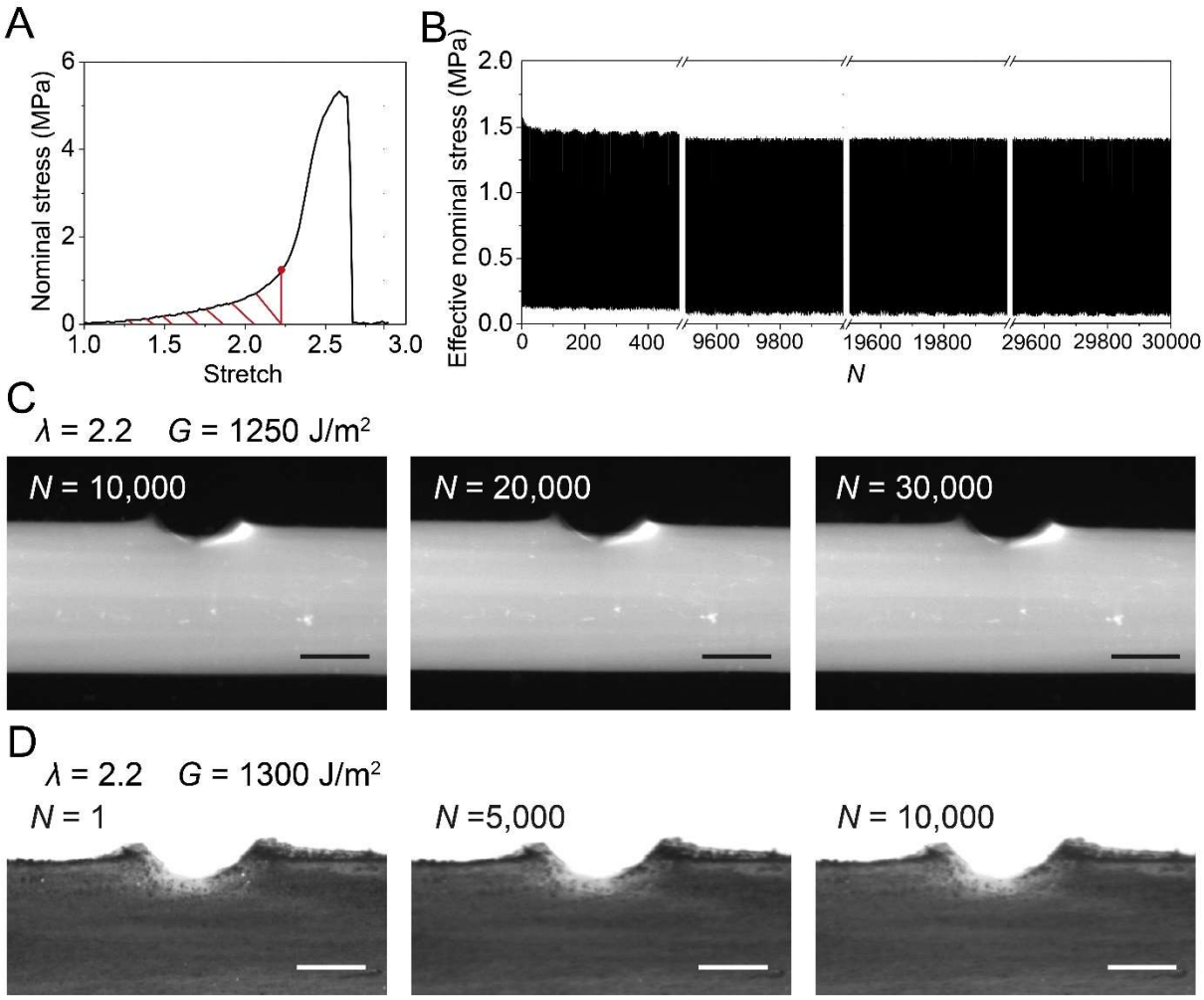

Fig. S10. Validation of high fatigue threshold of the prestretched PVA hydrogel. *(A)* Nominal stress versus stretch of the prestretched PVA hydrogel after prolonged cycles of 1000. The enclosed area indicated by red line denotes the strain energy at the applied stretch of 2.2, i.e., $W\left(\lambda = 2.2\right) = \int_1^{2.2} S d\lambda$. *(B)* The effective nominal stress $F/((W\text{-}c)t)$ versus cycle number N of the prestretched PVA hydrogel with a pre-crack c of 0.7 mm, where F is the measured force, W is the sample width, and t is the sample thickness. *(C)* Images of prestretched PVA hydrogel with a pre-crack at the applied energy release rate of 1250 J/m^2 at the cycle number of 10,000, 20,000, and 30,000. (D) Images of another prestretched PVA hydrogel with a pre-crack at the applied energy release rate of 1300 J/m^2 at the cycle number of 1, 5,000, and 10,000. High-contrast graphite

speckle patterns were applied to surfaces of samples, validating no observable crack propagation. Scale bars in *(C)* and (*D*) are 1 mm.

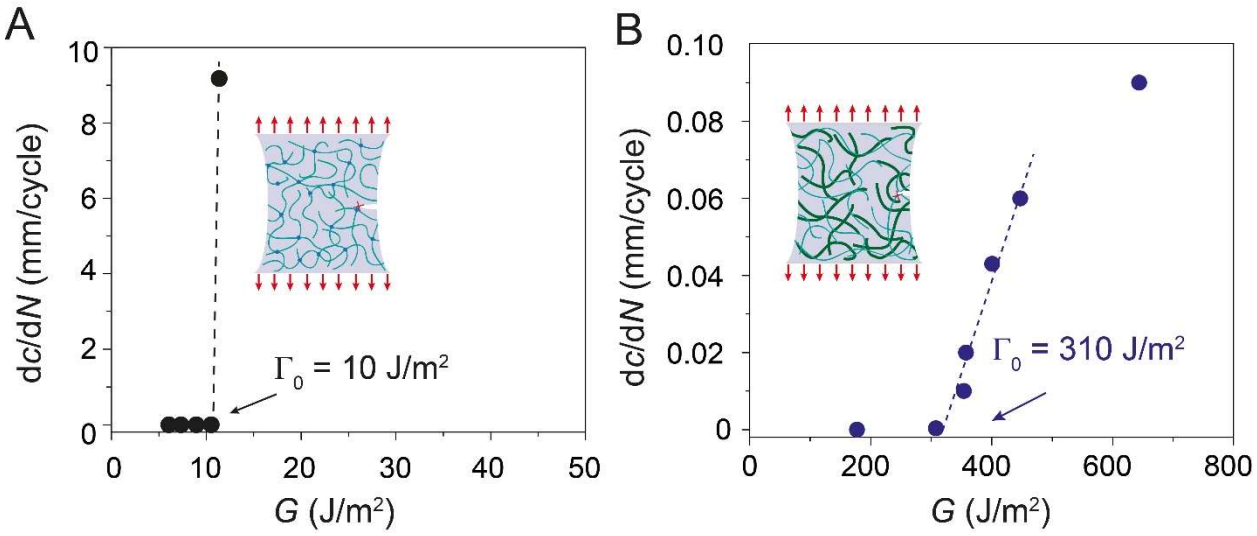

Fig. S11. Fatigue thresholds of PVA hydrogels. *(A)* Chemically cross-linked PVA hydrogel. *(B)* Freeze-thawed PVA hydrogel.

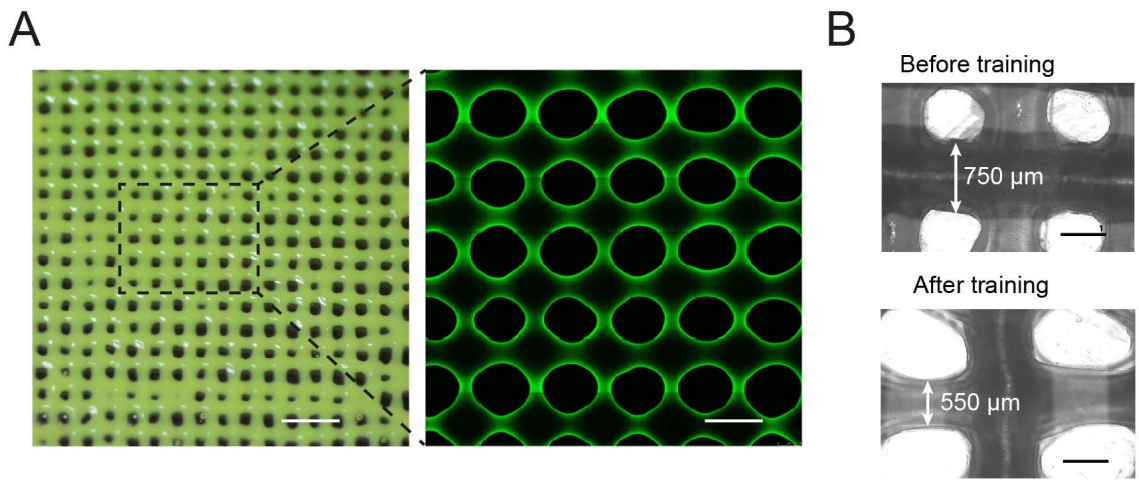

Fig. S12. 3D printing of PVA hydrogels into microstructures. *(A)* Optical image (left) and confocal image (right) of 3D printed PVA meshes (filling ratio: 50%). *(B)* Comparison of optical images of 3D printed mesh before and after mechanical training. Scale bars are 3 mm for left image and 500 µm for right image in *(A)*, 500 µm in *(B)*.

Legends for Supplementary Movie

Movie S1. Cyclic loading of the trained PVA mesh.

References

1. Yang W, *et al.* (2015) On the tear resistance of skin. *Nat Commun* 6:6649.
2. Lake G & Lindley P (1965) The mechanical fatigue limit for rubber. *J Appl Polym Sci* 9:1233-1251.
3. Wang Z, *et al.* (2019) Stretchable materials of high toughness and low hysteresis. *Proc Natl Acad Sci USA* 201821420.
4. Lin S, *et al.* (2019) Anti-fatigue-fracture hydrogels. *Sci Adv* 5:eaau8528.
5. Peppas NA & Merrill EW (1976) Differential scanning calorimetry of crystallized PVA hydrogels. *J. Appl. Polym. Sci.* 20:1457-1465.
6. Jaspers M, *et al.* (2014) Ultra-responsive soft matter from strain-stiffening hydrogels. *Nat Commun* 5:5808.
7. Kouwer PH, *et al.* (2013) Responsive biomimetic networks from polyisocyanopeptide hydrogels. *Nature* 493:651.
8. Vatankhah-Varnosfaderani M, *et al.* (2017) Mimicking biological stress–strain behaviour with synthetic elastomers. *Nature* 549:497.
9. Vatankhah-Varnosfaderani M, *et al.* (2018) Chameleon-like elastomers with molecularly encoded strain-adaptive stiffening and coloration. *Science* 359:1509-1513.
10. Sun J-Y, *et al.* (2012) Highly stretchable and tough hydrogels. *Nature* 489:133.
11. Gong JP, Katsuyama Y, Kurokawa T, & Osada Y (2003) Double-network hydrogels with extremely high mechanical strength. *Adv Mater* 15:1155-1158.
12. Huang Y, *et al.* (2017) Energy-dissipative matrices enable synergistic toughening in fiber reinforced soft composites. *Adv Funct Mater* 27:1605350.
13. Lin S, *et al.* (2014) Design of stiff, tough and stretchy hydrogel composites via nanoscale hybrid crosslinking and macroscale fiber reinforcement. *Soft Matter* 10:7519-7527.